The Journal of Chemical Physics

Simulation of the photodetachment spectrum of $HHfO^-$ using coupled-cluster calculations

Cite as: J. Chem. Phys. **145**, 244303 (2016); https://doi.org/10.1063/1.4972816
Submitted: 09 November 2016 . Accepted: 08 December 2016 . Published Online: 22 December 2016

Daniel K. W. Mok, John M. Dyke, and Edmond P. F. Lee

Simulation of the photodetachment spectrum of $HHfO^-$ using coupled-cluster calculations

Daniel K. W. Mok,[1] John M. Dyke,[2,a)] and Edmond P. F. Lee[1,2,a)]
[1]*Department of Applied Biology and Chemical Technology, The Hong Kong Polytechnic University, Hung Hom, Hong Kong*
[2]*School of Chemistry, University of Southampton, Highfield, Southampton SO17 1BJ, United Kingdom*

(Received 9 November 2016; accepted 8 December 2016; published online 22 December 2016)

The photodetachment spectrum of $HHfO^-$ was simulated using restricted-spin coupled-cluster single-double plus perturbative triple {RCCSD(T)} calculations performed on the ground electronic states of HHfO and $HHfO^-$, employing basis sets of up to quintuple-zeta quality. The computed RCCSD(T) electron affinity of 1.67 ± 0.02 eV at the complete basis set limit, including Hf $5s^25p^6$ core correlation and zero-point energy corrections, agrees well with the experimental value of 1.70 ± 0.05 eV from a recent photodetachment study [X. Li *et al.*, J. Chem. Phys. **136**, 154306 (2012)]. For the simulation, Franck-Condon factors were computed which included allowances for anharmonicity and Duschinsky rotation. Comparisons between simulated and experimental spectra confirm the assignments of the molecular carrier and electronic states involved but suggest that the experimental vibrational structure has suffered from poor signal-to-noise ratio. An alternative assignment of the vibrational structure to that suggested in the experimental work is presented. *Published by AIP Publishing.* [http://dx.doi.org/10.1063/1.4972816]

INTRODUCTION

Recently, Li *et al.*[1] reported the negative ion photoelectron (or photodetachment) spectra of ZrO^-, HfO^-, $HfHO^-$, and HfO_2H^-. This investigation is one of numerous, recent computational, and/or spectroscopic studies[2–10] published on the group IVB transition metal (Ti, Zr, and Hf) oxides, which have important industrial and technological applications, notably in catalytic processes, and the nuclear and electronics industries (see Refs. 1–10 and references therein). In Ref. 1, the photodetachment spectrum of $HfHO^-$ gave an electron affinity (EA) of 1.70 ± 0.05 eV, and the structural connectivity of HfHO and its anion were proposed to be H–Hf–O rather than Hf–O–H. The experimental spectrum showed a strong first component (the EA, labelled as A in Ref. 1) and two other weaker components to higher binding energy (labelled B and C). The A-B and B-C separations were measured as 730 cm^{-1}. To our knowledge, there are only two other studies available on HHfO. Both are infrared argon matrix studies,[11,12] which assign the observed vibrational absorptions of ~1627 and ~903 cm^{-1} to the HHf and HfO stretching modes of HHfO. Reference 11 also reported B3LYP geometry optimization and harmonic vibrational frequency calculations on HHfO and HfOH. The $^2A'$ state of HHfO was found to be the lowest energy minimum with the $^2\Delta$ and $^4\Sigma^-$ states of HfOH 12.6 and 42.1 kcal mol^{-1} higher in energy. The computed B3LYP harmonic frequencies of 1683 and 933 cm^{-1} for the HHf and HfO stretching modes of HHfO agree reasonably well with the above-mentioned IR absorptions.[11,12] However, the value of 730 cm^{-1}, the vibrational separations obtained from the photodetachment spectrum of $HHfO^-$,[1] is roughly halfway between the computed B3LYP HfO stretching (933 cm^{-1}) and HHfO bending (541 cm^{-1}) frequencies of HHfO ($^2A'$).[11] In order to confirm that the photodetachment spectrum reported by Li *et al.*[1] arises from $HHfO^-$ and to assign the vibrational structure, high level *ab initio* calculations on HHfO and its anion were carried out in the present study. Since the EA of HHfO has not been computed before, computing it with high level methods would assist the assignment of the observed photodetachment band to HHfO. Also, the photodetachment spectrum was simulated by computing Franck-Condon factors (FCFs) including allowances for anharmonicity and Duschinsky rotation.

COMPUTATIONAL DETAILS

Geometry optimization calculations were carried out on the $\tilde{X}^1A'$ state of $HHfO^-$ and the $\tilde{X}^2A'$ state of HHfO using the restricted-spin coupled-cluster single-double plus perturbative triple {RCCSD(T)} method,[13] as implemented in MOLPRO.[14] The different basis sets[15,16] and corresponding frozen cores employed are summarized in Table I. Harmonic vibrational frequencies of the $\tilde{X}^1A'$ state of $HHfO^-$ and the $\tilde{X}^2A'$ state of HHfO were computed at the RCCSD(T)/AVQZ level. In addition, geometry optimization calculations were performed on the $(1)^2A''$ state of HHfO at the RCCSD(T)/AVQZ level. Computed relative electronic energies (EAs) obtained at the RCCSD(T)/AwCVQZ and RCCSD(T)/AwCV5Z levels were extrapolated to the complete basis set (CBS) limit using the $1/X^3$ formula.[17]

222 and 240 RCCSD(T)/AwCV5Z energies were computed for the $\tilde{X}^1A'$ state of $HHfO^-$ and the $\tilde{X}^2A'$ state of HHfO,

a)Authors to whom correspondence should be addressed. Electronic addresses: jmdyke@soton.ac.uk and epl@soton.ac.uk

TABLE I. Basis sets used in RCCSD(T) calculations on $HHfO^-$/HHfO.

Labels	H and O	Hf	Nbasis[a]	Frozen core[b]
AVQZ	Aug-cc-pVQZ	Aug-cc-pVQZ_PP[c]	261	O $1s^2$ and Hf $5s^25p^6$
AwCVQZ	Aug-cc-pVQZ	Aug-cc-pwCVQZ_PP[c]	306	O $1s^2$
AwCV5Z	Aug-cc-pV5Z	Aug-cc-pwCV5Z_PP[c]	462	O $1s^2$

[a]Total number of contracted basis functions.
[b]With the AVQZ basis set, the default core was used; with the AwCVXZ, X = Q or 5, core,1,0 was used in the RCCSD(T) calculations (i.e., only the O $1s^2$ electron was frozen).
[c]The fully relativistic ECP60MDF effective core potential (ECP) was used to account for the $1s^22s^22p^63s^23p^63d^{10}4s^24p^64d^{10}4f^{14}$ core electrons of Hf, with the associated basis sets shown in the table to account for the $5s^25p^66s^25d^2$ electrons of Hf.

respectively. They were each fitted to potential energy functions (PEFs; see the supplementary material for details).[18,19] Anharmonic vibrational wavefunctions and energies were computed employing these PEFs, which were then used to calculate FCFs including anharmonicity and Duschinsky rotation, as described previously.[18–20] Each vibrational component of the $(\tilde{X}^2A')$ HHfO + e ← $(\tilde{X}^1A')$ $HHfO^-$ ionization was simulated employing the computed anharmonic FCF with a Gaussian line shape and various full-width-at-half-maximum (FWHM) values. The experimental EA value was used in the simulated spectra for the ease of comparison with the experimental spectrum.

TABLE II. Optimized geometrical parameters {HHf and HfO bond lengths in Å and HHfO (θ) bond angle in degrees}, computed vibrational frequencies {harmonic, ω, and fundamental, (ν), in cm^{-1}}, and electron affinities (EA in eV) of $HHfO^-$/HHfO obtained from RCCSD(T) calculations using different basis sets.[a]

$HHfO^-$ $\tilde{X}^1A'$	HHf	HfO	θ	$\omega_1/(\nu_1)$	$\omega_2/(\nu_2)$	$\omega_3/(\nu_3)$	EA
AVQZ	1.9415	1.7850	108.738	1431	865	467	
AwCVQZ	1.9201	1.7575	107.928				
AwCV5Z	1.9183	1.7557	107.873				
AwCV5Z PEF[b]	1.9149	1.7555	107.857	1453.3[c]	891.6[c]	479.9[c]	
				(1394.2)[c]	(884.9)[c]	(469.0)[c]	
				1453.3[d]	891.9[d]	479.9[d]	
				(1394.3)[d]	(885.2)[d]	(469.0)[d]	
HHfO $\tilde{X}^2A'$							
AVQZ	1.8738	1.7514	107.169	1649.0	926.2	502.8	1.673
AVQZ (EA_0)[e]							1.693
AwCVQZ	1.8487	1.7266	105.115				1.615
AwCV5Z//AwCVQZ							1.631
AwCV5Z	1.8476	1.7248	105.033				1.631
AwCV5Z PEF[b]	1.8456	1.7239	104.901	1681.1[c]	948.5[c]	517.2[c]	1.631
				(1639.2)[c]	(940.8)[c]	(505.4)[c]	
				1681.1[d]	948.9[d]	517.2[d]	
AwCV5Z PEF[b] (EA_0)[f]				(1626.7)[d]	(941.1)[d]	(505.4)[d]	1.651
CBS$(1/X^3)$[g]							1.647 ± 0.016
CBS$(1/X^3)$[g] (EA_0)[h]							1.67 ± 0.02
B3LYP[i]	1.831	1.744	102.4	1683	933	541	
IR matrix (Ar)[i]				(1626.5)	(902.9)		
IR matrix (Ar)[j]				(1626.7)	(902.7)		
Photodetachment[k]					(730)		1.70 ± 0.05
HHfO $(1)^2A''$							
AVQZ	1.8500	1.9946	117.733				4.942

[a]See Table I for the basis sets used; ω_1, ω_2, and ω_3 correspond to the HHf stretching, HfO stretching, and HHfO bending modes, respectively.
[b]From fitting of the potential energy function.
[c]Using the atomic mass of 177.943 696 for the most abundant (38.08%) isotope of ^{178}Hf.
[d]Using the average atomic mass of 178.49 for Hf.
[e]EA_0 is the zero-point energy (ZPE) corrected RCCSD(T)/AVQZ EA value using the computed RCCSD(T)/AVQZ harmonic vibrational frequencies.
[f]EA_0 is the zero-point energy (ZPE) corrected RCCSD(T)/AwCV5Z EA value using the computed RCCSD(T)/AwV5Z fundamental vibrational frequencies (ΔZPE = 0.020 eV).
[g]The CBS value is obtained using the $1/X^3$ extrapolation formula with the RCCSD(T)/AwCV5Z and RCCSD(T)/AwCVQZ EA values; the estimated uncertainties are based on the difference between the RCCSD(T)/CBS and RCCSD(T)/AwCV5Z value.
[h]EA_0 is the zero-point energy corrected RCCSD(T)/CBS EA value using the computed RCCSD(T)/AwV5Z fundamental vibrational frequencies.
[i]From Ref. 11: B3LYP calculations employing the 6-311++G** basis set for H and O and the Los Alamos ECP plus DZ basis sets for Hf; IR matrix of laser-ablated Hf + H_2O.
[j]From Ref. 12: IR matrix of laser-ablated Hf + H_2O_2.
[k]From Ref. 1: Mass selected anion photodetachment of laser vaporization of the oxide on the surface of a hafnium rod.

RESULTS AND DISCUSSION

Optimized geometrical parameters, computed harmonic and fundamental vibrational frequencies, and computed EAs obtained at different levels of calculation are summarized in Table II. First, the $(1)^2A''$ state of HHfO, which has not been studied previously, has a computed EA of 4.94 eV at the RCCSD(T)/AVQZ level. Since this value is considerably larger than the photon energy of 3.45 eV used in Ref. 1 to record their photodetachment spectra, this electronic state will not be further discussed.

From Table II, it can be seen that there are relatively large differences between the optimized geometrical parameters obtained with the default frozen core using the AVQZ basis set and with the Hf $5s^25p^6$ core electrons included in the correlation calculation using the AwCVXZ, X = Q or 5, basis sets. Specifically, the largest differences in the computed bond lengths and angles between using the AVQZ and AwCVQZ basis sets are 0.0275 Å for r(HfO) of $HHfO^-$ and 2.054° for θ(HHfO) of HHfO. The corresponding computed EAs differ by 0.058 eV. These comparisons show significant Hf $5s^25p^6$ core correlation effects. Nevertheless, when the Hf $5s^25p^6$ electrons were correlated, the differences in the results obtained between using the AwCVQZ and AwCV5Z basis sets are small. Specifically, the largest differences in the computed bond lengths, bond angles, and EAs are 0.002 Å for r(HHf) of HHfO, 0.055° for θ(HHfO) of $HHfO^-$, and 0.016 eV, respectively. These comparisons suggest that the AwCV5Z results are near the CBS limit. Comparing with the B3LYP results of Ref. 1, the RCCSD(T)/AwCV5Z r(HHf) and r(HfO) bond lengths of HHfO obtained in the present study are 0.0166 Å larger and 0.0192 Å smaller than the corresponding B3LYP values, respectively, and the RCCSD(T)/AwCV5Z bond angle is 2.633° larger than the B3LYP value. These comparisons suggest that the B3LYP geometrical parameters are not very reliable, especially the bond angle. Regarding relative energies, the best computed EA_0 (EA including zero-point-energy (ZPE) corrections) value of 1.67 ± 0.02 eV obtained here at the RCCSD(T)/CBS level, including Hf $5s^25p^6$ core correlation and zero-point energy (ZPE) corrections (Table II), agrees very well with the experimental value of 1.70 ± 0.05 eV from Ref. 1, confirming the molecular carrier to be $HHfO^-$ and also the electronic states of HHfO and $HHfO^-$ involved.

Regarding the computed vibrational frequencies of the $\tilde{X}^1A'$ state of $HHfO^-$ and the $\tilde{X}^2A'$ state of HHfO obtained using the PEFs computed in the present study, we have used the atomic mass of 177.943696 for the most abundant (38.08%) isotope of ^{178}Hf and also the average atomic mass of 178.49 for Hf (footnotes c and d of Table II) in the calculation of the anharmonic vibrational wavefunctions and energies. In practice, the differences in the computed vibrational frequencies between using the two atomic masses of Hf, as shown in Table II, are negligibly small, except for the computed HHf fundamental frequencies of HHfO (*vide infra*). Hence, from here onward, vibrational results to be discussed are those obtained using the average atomic mass of Hf. From Table II, as shown by the differences between the computed harmonic and fundamental frequencies obtained in the present study, anharmonic effects are significant, especially for the HHf stretching modes of both HHfO and $HHfO^-$ as expected. For HHfO, some experimental fundamental vibrational frequencies are available from two IR studies.[11,12] It is pleasing to see that the computed HHf stretching fundamental frequency of HHfO, 1626.7 cm^{-1}, obtained with the average atomic mass of Hf (cf. 1639.2 cm^{-1} with ^{178}Hf) in the present study, is almost identical with the available experimental IR values[11,12] (~1627 cm^{-1}; see Table II). For the HfO stretching mode of HHfO, our computed fundamental frequency (941 cm^{-1}) is slightly larger than the computed B3LYP harmonic value (933 cm^{-1}) and the IR values (~903 cm^{-1}). The value of 730 cm^{-1} obtained from the vibrational separations in the photodetachment spectrum[1] of $HHfO^-$ is still roughly halfway between the computed fundamental frequencies of the HfO stretching and bending modes (941 and 505 cm^{-1}) obtained here for HHfO. This is discussed further, when the vibrational structures of simulated and experimental photodetachment spectra are compared below.

Some simulated photodetachment spectra of $HHfO^-$ obtained at the Boltzmann vibrational temperatures of 0, 300, and 500 K with different FWHMs (5 or 35 meV) are shown in Figure 1. The simulated spectrum at 1000 K with a FWHM of 35 meV is given in the supplementary material (Figure S1, bottom trace; the top trace is the experimental spectrum of Ref. 1). The simulated photodetachment spectrum at 500 K with a FWHM of 40 meV is shown in Figure 2 (bottom trace). This simulated spectrum is considered as having the best match with the experimental spectrum[1] (Figure 2, top trace). Computed FCFs, as bar diagrams, with some major vibrational assignments are given in Figure S2 (supplementary material). The comparison between the best simulated and experimental spectrum in Figure 2 shows a reasonably good agreement

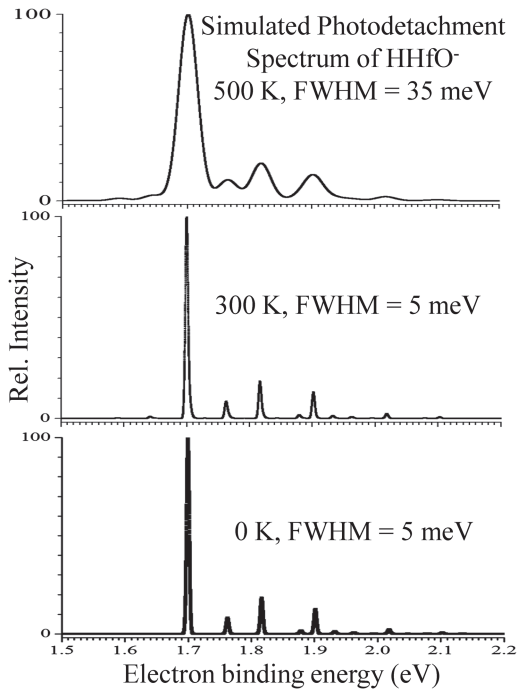

FIG. 1. Simulated photodetachment spectra for the HHfO ($\tilde{X}^2A'$) + e ← $HHfO^-$ ($\tilde{X}^1A'$) ionization at Boltzmann vibrational temperatures of 500 K (FWHM = 35 meV; top), 300 K (FWHM = 5 meV; middle), and 0 K (FWHM = 5 meV; bottom).

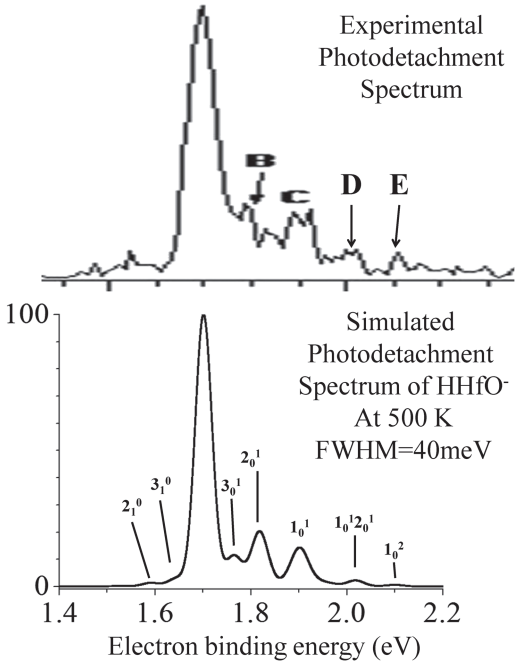

FIG. 2. Comparison between the simulated (bottom) and experimental (top; from Ref. 1) photodetachment spectra of $HHfO^-$; the simulated spectrum has a Boltzmann vibrational temperature of 500 K and a FWHM of 40 meV.

in the overall vibrational structure. Specifically, both have a very strong (0,0,0)-(0,0,0) (or 0_0^0) vibrational component and roughly the same overall energy spread (~1.6 to ~2.2 eV). Therefore, it is concluded that the simulated spectrum also supports the assignments of the molecular carrier and the electronic states involved.

Before the weak experimental vibrational structure in the "hot band" and/or higher electron binding energy (EBE; above the main EA component) region is compared with the simulated spectrum, it should be noted that the signal to noise level shown in the 1.4–1.6 and >2.2 eV EBE regions of the experimental spectrum[1] (Figure 2, top trace) is rather poor especially for the weak vibrational structure. Also, the vibrational features, labelled as B and C in the experimental spectrum, are clearly poorly resolved. In this connection, the $A(0_0^0)$-B and B-C vibrational separations of 730 cm^{-1} reported in Ref. 1 are likely to be inaccurate. In addition, the poor signal-to-noise of the experimental spectrum suggests a weak $HHfO^-$ anion beam. In this connection, the "noisy" vibrational features of B and C may also be due to instability of the anion beam.

When the simulated and experimental weak vibrational features are compared, the following points are noted. First, the simulated 2_1^0 and 3_1^0 "hot bands" at a vibrational temperature of 500 K are at 1.59 and 1.64 eV (Figure 2, bottom). This and other simulated spectra with different vibrational temperatures and resolutions (FWHMs; Figure 1 and especially Figure S1 of the supplementary material) suggest that "hot bands" in the experimental spectrum cannot be strong and the vibrational temperature is at most ~500 K. The weak features in the 1.40 to ~1.55 eV EBE region of the experimental spectrum cannot be due to "hot bands," but are just background noise, similar to that in the >2.2 eV region. Second, with vibrational separations of 730 cm^{-1} reported in Ref. 1, the spectral feature C has an EBE of 1.88 eV. Comparing with the simulated spectrum (Figure 2, bottom trace), feature C in the experimental spectrum is mainly due to the 1_0^1 vibrational component with a computed EBE of 1.90 eV (with the 0_0^0 peak set to 1.70 eV; see also Figure S2 of the supplementary material). Third, labels D and E were added in the experimental spectrum (Figure 2, top trace) to indicate two weak features in the 2.0 to 2.1 eV region. Features D and E can be assigned to the $1_0^1 2_0^1$ and 1_0^2 vibrational components with computed EBE values of 2.02 and 2.10 eV, respectively. Last, using the vibrational separations of 730 cm^{-1} given in Ref. 1, the EBE position of feature B, as indicated by the "arrow" shown in Figure 2 (top trace), is 1.79 eV. Feature B in the experimental spectrum clearly shows some sub-structure, though this may not be reliable because of poor signal to noise ratio of the spectrum. Nevertheless, comparing with the simulated vibrational structure, the sub-structure in feature B may be assigned to the 3_0^1 and 2_0^1 vibrational components at 1.76 and 1.82 eV, respectively. Summarizing, the spectrum assignment to $HHfO^-$ has been confirmed, and based on our simulated vibrational structure, more detailed and credible assignments of the experimental vibrational structure in the photodetachment spectrum of $HHfO^-$ than given in Ref. 1 have been proposed.

CONCLUSION

High level *ab initio* calculations were carried out on the ground electronic states of HHfO and its anion, and FCFs between the two states involved were computed including allowances for anharmonicity and Duschinsky rotation, for the first time. Computed anharmonic FCFs were used to simulate the photodetachment spectrum of $HHfO^-$. The good agreement between the computed and experimental EA_0 values, and between the overall simulated and experimental vibrational structures, confirms the assignment of the experimental photodetachment spectrum of Ref. 1 to be due to the HHfO ($\tilde{X}^2A'$) + e ← $HHfO^-$ ($\tilde{X}^1A'$) ionization. Based on our simulated vibrational structure, new and more detailed assignments of the observed vibrational structure have been proposed. In this connection, we suggest further spectroscopic investigations on the photodetachment spectrum of $HHfO^-$.

SUPPLEMENTARY MATERIAL

See supplementary material for the potential energy functions (PEFs) of the $\tilde{X}^1A'$ state of $HHfO^-$ and the $\tilde{X}^2A'$ state of HHfO, the simulated photodetachment spectrum of $HHfO^-$ at a Boltzmann vibrational temperature of 1000 K with a FWHM of 35 meV (Figure S1), and some major computed Franck-Condon factors (FCFs) for the HHfO ($\tilde{X}^2A'$) + e ← $HHfO^-$ ($\tilde{X}^1A'$) ionization at Boltzmann vibrational temperatures of 500 (bottom) and 300 (top) K, and some major vibrational assignments (Figure S2).

ACKNOWLEDGMENTS

The authors are grateful to the RGC of HKSAR (GRF Grant Nos. PolyU 5018/13P and PolyU 153013/15P) for support. Computations were carried out using resources of the NSCCS, EPSRC (UK).

[1]X. Li, W. Zheng, A. Buonaugurio, A. Buytendyk, K. Bowen, and K. Balasubramanian, J. Chem. Phys. **136**, 154306 (2012).
[2]D. K. W. Mok, F.-t. Chau, J. M. Dyke, and E. P. F. Lee, Chem. Phys. Lett. **458**, 11 (2008).
[3]D. K. W. Mok, E. P. F. Lee, F.-t. Chau, and J. M. Dyke, Phys. Chem. Chem. Phys. **10**, 7270 (2008).
[4]H.-J. Zhai, W.-J. Chen, S.-J. Lin, X. Huang, and L.-S. Wang, J. Phys. Chem. A **117**, 1042 (2013).
[5]J. B. Kim, M. L. Weichman, and D. M. Neumark, Phys. Chem. Chem. Phys. **15**, 20973 (2013).
[6]Y.-C. Chou, Comput. Theor. Chem. **1069**, 112 (2015).
[7]Y.-C. Chang, H. Huang, Z. Luo, and C. Y. Ng, J. Chem. Phys. **138**, 041101 (2013).
[8]X. Zhuang, A. Le, T. C. Steimle, R. Nagarajan, V. Guptab, and J. P. Maier, Phys. Chem. Chem. Phys. **12**, 15018 (2010).
[9]F. Grein, J. Chem. Phys. **126**, 034313 (2007).
[10]S. Li and D. A. Dixon, J. Phys. Chem. A **114**, 2665 (2010).
[11]M. Zhou, L. Zhang, J. Dong, and Q. Qin, J. Am. Chem. Soc. **122**, 10680 (2000).
[12]X. Wang and L. Andrews, Inorg. Chem. **44**, 7189 (2005).
[13]P. J. Knowles, C. Hampel, and H.-J. Werner, J. Chem. Phys. **99**, 5219 (1993); Erratum, **112**, 3106 (2000).
[14]H.-J. Werner, P. J. Knowles, G. Knizia, F. R. Manby, M. Schütz, P. Celani, W. Györffy, D. Kats, T. Korona, R. Lindh, A. Mitrushenkov, G. Rauhut, K. R. Shamasundar, T. B. Adler, R. D. Amos, A. Bernhardsson, A. Berning, D. L. Cooper, M. J. O. Deegan, A. J. Dobbyn, F. Eckert, E. Goll, C. Hampel, A. Hesselmann, G. Hetzer, T. Hrenar, G. Jansen, C. Köppl, Y. Liu, A. W. Lloyd, R. A. Mata, A. J. May, S. J. McNicholas, W. Meyer, M. E. Mura, A. Nicklass, D. P. O'Neill, P. Palmieri, D. Peng, K. Pflüger, R. Pitzer, M. Reiher, T. Shiozaki, H. Stoll, A. J. Stone, R. Tarroni, T. Thorsteinsson, and M. Wang, MOLPRO, version 2015.1, a package of *ab initio* programs, 2015, see http://www.molpro.net.
[15]D. Figgen, K. A. Peterson, M. Dolg, and H. Stoll, J. Chem. Phys. **130**, 164108 (2009).
[16]T. H. Dunning, Jr., J. Chem. Phys. **90**, 1007 (1989).
[17]A. Halkier, T. Helgaker, W. Klopper, P. Jorgensen, and A. G. Császár, Chem. Phys. Lett. **310**, 385 (1999).
[18]D. K. W. Mok, E. P. F. Lee, F.-T. Chau, and J. M. Dyke, J. Chem. Phys. **120**, 1292 (2004).
[19]E. P. F. Lee, D. K. W. Mok, F.-T. Chau, and J. M. Dyke, J. Chem. Phys. **127**, 214305 (2007).
[20]F.-T. Chau, D. K. W. Mok, E. P. F. Lee, and J. M. Dyke, J. Chem. Phys. **121**, 1810 (2004).